Konrad-Zuse-Zentrum
für Informationstechnik Berlin

Takustraße 7
D-14195 Berlin-Dahlem
Germany

DANIEL RUPRECHT RUPERT KLEIN ANDREW J. MAJDA

Moisture-Gravity Wave Interactions in a Multiscale Environment

ZIB-Report 09-21 (Juni 2009)

MOISTURE-GRAVITY WAVE INTERACTIONS IN A MULTISCALE ENVIRONMENT

DANIEL RUPRECHT*, RUPERT KLEIN*, AND ANDREW J. MAJDA†

Abstract. Starting from the conservation laws for mass, momentum and energy together with a three species, bulk microphysic model, a model for the interaction of internal gravity waves and deep convective hot towers is derived by using multiscale asymptotic techniques.

From the resulting leading order equations, a closed model is obtained by applying weighted averages to the smallscale hot towers without requiring further closure approximations. The resulting model is an extension of the linear, anelastic equations, into which moisture enters as the area fraction of saturated regions on the microscale with two way coupling between the large and small scale. Moisture reduces the effective stability in the model and defines a potential temperature sourceterm related to the net effect of latent heat release or consumption by microscale up- and downdrafts.

The dispersion relation and group velocity of the system is analyzed and moisture is found to have several effects: It reduces energy transport by waves, increases the vertical wavenumber but decreases the slope at which wave packets travel and it introduces a lower horizontal cutoff wavenumber, below which modes turn into evanescent. Further, moisture can cause critical layers.

Numerical examples for steadystate and timedependent mountain waves are shown and the effects of moisture on these waves are investigated.

1. Introduction. Internal gravity waves are the prominent feature of atmospheric flows on lengthscales reaching from 10 to the order of 100km. Although they are not resolved in General Circulation Models (GCM), their effects are important to capture by parameterizations to obtain realistic flows. The development of such parameterizations usually relies on physical arguments, leading to simplified models for the process to parameterize. Multiscale asymptotics can be used as a tool to derive such models in a more systematic way, a strategy discussed for example in [18] and [14].

This paper is based on the model for fast gravity waves (timescale of ~ 100s) in a deep convective, hot tower regime that is derived in [15]. Using a slightly extended ansatz, allowing for a constant background flow, the same steps described there are repeated and a brief recapitulation of the key steps is given. The main parts of the paper at hand are first the derivation of a closed set of equations out of the leading order equations emerging from the multiscale analysis and second an investigation of some properties of this model and a comparison to the dry case.

The resulting model is an extension of the linear, anelastic equations. It contains a mechanism for the reduction of the stability frequency by averaged moist dynamics and includes two additional equations for the averaged perturbation vertical velocity and potential temperature. These equations will define a sourceterm for the largescale potential temperature related to moist dynamics of the perturbation quantities. Also, the largescale flow does enter the equations for the perturbation quantities, so that there is a bidirectional coupling between large- and smallscale equations.

In [3] a model for steady, moist, hydrostatic flow over a mountain with reversible moist dynamics is proposed. The model distinguishes between saturated and nonsaturated regions by a switching function that depends on the vertical displacement of a parcel: if the parcel is displaced beyond the lifting condensation level it is treated as saturated and the dry stability frequency is replaced by the moist stability frequency. Although being distinctively different, the model derived in the paper at hand has

*FB Mathematik, Freie Universität Berlin, Arnimallee 6, 14195 Berlin, Germany E-mail: ruprecht@zib.de. Supported by the DFG MetStroem SPP 1276 and PGP SSP 1167

†Courant Institute of Mathematical Sciences, New York University

certain similiarities worth pointing out: it also employs a switching function distinguishing between saturated and nonsaturated regions, but the switch does directly depend on the mixing ratio of watervapor. Further, because the model is based on an ansatz with two horizontal scales, the stability frequency not only changes between moist and dry but is modified in a continous way, depending on the area fraction of saturated regions on the small scale.

In [2] their model is extended to nonhydrostatic flow with irreversible condensation and in [1] to nonlinear, steady flow. It is found that moisture adjacent to the ground can significantly reduce the mountain drag, a result also found in the examples investigated in the paper at hand.

In [13], nonlinear, nonsteady, nonhydrostatic anelastic flows are investigated. Here, the mixing ratios of liquid water and vapor are treated as prognostic variables, defining heating source terms for the potential temperature. Besides finding again that moisture can reduce drag, it is also found that moisture does reduce the wave intensity and steepens the resulting wave patterns. While the first result is also found in the examples in this paper, instead of a steepening of patterns, a reduction of the propagation angle is observed in the presented examples.

[7] employ a fully compressible model combined with prognostic equations for watervapor, rainwater and cloudwater to simulate moist mountain waves. They also find that moisture reduces the vertical flux of horizontal momentum and the amplitude of the generated wave patterns. Also, they observe an increase in vertical wavelength for nearly hydrostatic waves. Attenuation of gravity waves by moisture and an increase of vertical wavelength was also found in the analysis of wave propagation in a fully saturated atmosphere in [8]. Note that all these models employ explicit closures, while the model presented in the paper at hand features an analytic mass flux closure.

This paper is organized as follows: In 2, first the Ansatz for the derivation in [15] is briefly reviewed and extended by a constant, horizontal background wind. Then the main part in that section is the analytic derivation of a closed set of equations out of this model. In 3, some properties of the resulting set of equations are pointed out, for example the dispersion relation and the group velocity, and compared to the dry case. Section 4 demonstrates the effect of moisture in some numerical examples.

2. Derivation of the model. The derivation in [15] is based on a distinguished limit for Mach-, barotropic Froude- and bulk microscale Rossby number connected by a generic asymptotic expansion parameter ε:

$$\mathrm{M} \sim \overline{\mathrm{Fr}} \sim \varepsilon^2, \quad \mathrm{Ro_B} \sim \varepsilon^{-1} \quad \text{as } \varepsilon \to 0 \tag{2.1}$$

See [14] for a detailed explanation of this technique. The starting point of the model development are the conservation laws for momentum, mass and energy combined with a slightly modified version of the bulk microphysics model described in [12]. The prognostic quantities in the original equations are horizontal velocity $\vec{u}$, vertical velocity w, density ρ, pressure p, potential temperature θ and the mixing ratios of water vapor q_v, cloud water q_c and rain water q_r.

The scales at which the model is focussed are a timescale of $\tau_\mathrm{ref} \approx 100\mathrm{s}$, a vertical length scale equal to the pressure scale height $z_\mathrm{ref} = h_\mathrm{sc} \approx 10\mathrm{km}$ and two horizontal scales $x_\mathrm{ref} \approx 10\mathrm{km}$ and $\eta_\mathrm{ref} \approx 1000\mathrm{m}$. These scales are connected to the universal reference quantities for time, length and velocity derived in [14] by the expansion parameter

$$\begin{aligned} &\tau \approx \varepsilon^{-1} t_{\text{ref}} \ , \ x \approx h_{\text{sc}} \ , \ \eta \approx \varepsilon^{-1} h_{\text{sc}} \\ &z \approx h_{\text{sc}} \ , \ u \approx u_{\text{ref}} \ , \end{aligned} \tag{2.2}$$

The small horizontal scale η resolves the horizontal variation inside deep moist convective towers that are common in the tropics. The timescale τ corresponds to the advection timescale of this smaller lengthscale while the larger scales x and z describe the regime of nonrotating and nonhydrostatic gravity waves. Note that the reference frequency set by the timescale is 0.01s^{-1} and thus compatible with the typical value used for the stability or Brunt-Väisälä frequency. Further, it is assumed that the horizontal velocity is independent of the small horizontal scale η.

The model distinguishes between saturated and nonsaturated areas by a switching function H_{q_v} defined as a function of the leading order water vapor content:

$$H_{q_v}(q_v^{(0)}(\mathbf{x},\eta,z,\tau)) = \begin{cases} 1 & : \quad q_{\text{v}}^{(0)}(\mathbf{x},\eta,z,\tau) \geq q_{\text{vs}}^{(0)}(z) \quad \text{(saturation)} \\ 0 & : \quad q_{\text{v}}^{(0)}(\mathbf{x},\eta,z,\tau) < q_{\text{vs}}^{(0)}(z) \quad \text{(undersaturation)} \end{cases} \tag{2.3}$$

Here, q_{vs} is the saturation water vapor mixing ratio computed from Boltons formula for saturation vapor pressure (see [9] for the formula and [15] for the derivation of an expression for q_{vs}).

Here, we slightly modify the ansatz for the horizontal velocity by introducing a constant background velocity u^∞. To avoid inconsistencies in the derivation, we also need to add a second timescale τ', corresponding to the timescale set by advection of flows with u^∞-velocity over η-distances. The terms related to τ' will eventually drop out by sublinear growth conditions in the end and will not appear in the final model. In terms of ε the timescale is

$$\tau' \approx \varepsilon^{-2} t_{\text{ref}} \tag{2.4}$$

and so the ansatz for horizontal velocity now is

$$u(x,z,t;\varepsilon) = \varepsilon^{-1} u^\infty + u^{(0)}(x,z,\tau) + \mathcal{O}(\varepsilon) \tag{2.5}$$

Note that as $\varepsilon \approx 0.1$ and $u_{\text{ref}} = 10\text{m/s}$, a dimensional background flow of 10m/s corresponds to a nondimensional value of $u^\infty = 0.1$ and this value will be used in most of the numerical examples presented later. The expansions of the other dynamical quantities as well as the moist variables are as described in [15] except that all quantities depending on τ now also depend on τ'.

All quantities are split up as

$$\phi = \overline{\phi} + \tilde{\phi} \tag{2.6}$$

with

$$\bar{\phi} = \lim_{\eta_0 \to \infty} \frac{1}{2\eta_0} \int_{-\eta_0}^{\eta_0} \phi(\eta) d\eta \tag{2.7}$$

denoting the average over η while the tilde part are perturbations from this average. We present the model derivation in a x-z-plane here. On the one hand, this simplifies the notation, on the other hand the presented numerical examples will be of this type, too.

The leading order equations for the averages resulting from this ansatz are

$$\begin{aligned}
\bar{u}^{(0)}_\tau + u^\infty \bar{u}^{(0)}_x + \pi^{(3)}_x &= 0 \\
\bar{w}^{(0)}_\tau + u^\infty \bar{w}^{(0)}_x + \pi^{(3)}_z &= \bar{\theta}^{(3)} \\
\bar{\theta}^{(3)}_\tau + u^\infty \bar{\theta}^{(3)}_x + \bar{w}^{(0)}\theta^{(2)}_z &= \frac{\Gamma^{**} L^{**} q^{**}_{\mathrm{vs}}}{p_0} \left(\overline{H_{q_v} C^{(0)}_{\mathrm{d}}} + \overline{(H_{q_v} - 1)\, C^{(0)}_{\mathrm{ev}}} \right) \\
\left(\rho^{(0)} \bar{u}\right)_x + \left(\rho^{(0)} \bar{w}\right)_z &= 0
\end{aligned} \tag{2.8}$$

with $\pi^{(3)} = p^{(3)}/\rho^{(0)}$ and $\theta^{(2)}_z(z)$ being the moist adiabatic potential temperature gradient of the background, $C^{(0)}_{\mathrm{d}}$ the leading order sourceterm from vapor condensating to cloudwater or cloudwater evaporating and $C^{(0)}_{\mathrm{ev}}$ the leading order sourceterm representing cooling by evaporating rain. The equations for the perturbations read

$$\begin{aligned}
\tilde{w}^{(0)}_\tau + u^\infty \tilde{w}^{(0)}_x + u^{(0)} \tilde{w}_\eta &= \tilde{\theta}^{(3)} \\
\tilde{\theta}^{(3)}_\tau + u^\infty \tilde{\theta}^{(3)}_x + u^{(0)} \tilde{\theta}^{(3)}_\eta + \tilde{w}^{(0)} \theta^{(2)}_z &= \\
\frac{\Gamma^{**} L^{**} q^{**}_{\mathrm{vs}}}{p_0} \left(H_{q_v} C^{(0)}_{\mathrm{d}} - \overline{H_{q_v} C^{(0)}_{\mathrm{d}}} \; + \; (H_{q_v} - 1)\, C^{(0)}_{\mathrm{ev}} - \overline{(H_{q_v} - 1)\, C^{(0)}_{\mathrm{ev}}} \right)
\end{aligned} \tag{2.9}$$

The resulting leading order equations for the moist species split into the saturated ($H_{q_v} = 1$) and the undersaturated ($H_{q_v} = 0$) case

Saturated.

$$\begin{aligned}
-\left(\bar{w}^{(0)} + \tilde{w}^{(0)}\right) q^{(0)}_{\mathrm{vs,z}} &= C^{(0)}_{\mathrm{d}} \\
q^{(0)}_{\mathrm{r},\tau} + u^\infty q^{(0)}_{\mathrm{r,x}} + u^{(0)} q^{(0)}_{\mathrm{r},\eta} &= 0
\end{aligned} \tag{2.10}$$

Undersaturated.

$$\begin{aligned}
C^{**}_{\mathrm{ev}} \left(q^{(0)}_{\mathrm{vs}} - q^{(0)}_{\mathrm{v}} \right) \sqrt{q^{(0)}_{\mathrm{r}}} &= C^{(0)}_{\mathrm{ev}} \\
q^{(0)}_{\mathrm{v},\tau} + u^\infty q^{(0)}_{\mathrm{v,x}} + u^{(0)} q^{(0)}_{\mathrm{v},\eta} &= 0 \\
q^{(0)}_{\mathrm{r},\tau} + u^\infty q^{(0)}_{\mathrm{r,x}} + u^{(0)} q^{(0)}_{\mathrm{r},\eta} &= 0
\end{aligned} \tag{2.11}$$

The keysteps of the derivation can be found in the appendix.

2.1. Computing the massflux closure. To obtain a closed set of equations, an expression for the averaged moisture related sourceterm in the equation for $\bar{\theta}^{(3)}$ in (2.8) will be derived out of the perturbation equations (2.9) and the leading order equations (2.10) and (2.11) obtained from the bulk microscale model. The derivation will be purely analytically and does not require additional physical assumptions.

Multiply the equation for $C^{(0)}_{\mathrm{d}}$ in (2.10) by $H_{q_{\mathrm{v}}}$ and average over η to get

$$-\overline{H_{q_{\mathrm{v}}}} \bar{w}^{(0)} q^{(0)}_{\mathrm{vs},z} - \overline{H_{q_{\mathrm{v}}} \tilde{w}^{(0)}} q^{(0)}_{\mathrm{vs},z} = \overline{H_{q_{\mathrm{v}}} C^{(0)}_{\mathrm{d}}} \tag{2.12}$$

Looking at the transport equations for watervapor (2.11) and noting that in the saturated region, $q^{(0)}_{\mathrm{v}} = q^{(0)}_{\mathrm{vs}}(z)$ trivially satisfies the same transport equation, it is

$$q^{(0)}_{\mathrm{v}}(x, z, \eta, \tau) = q^{(0)}_{\mathrm{v}}(x - u^\infty \tau, z, \eta - \int_0^\tau u^{(0)}(x, z, t')dt', 0) \tag{2.13}$$

Now define

$$\sigma(x,z,\tau) := \overline{H_{\mathrm{q_v}}(x,z,\eta,\tau)} \tag{2.14}$$

As $\int_0^\tau u^{(0)}(x,z,t')dt'$ is independent of η, we get

$$\begin{aligned}\sigma(x,z,\tau) &= \overline{H_{\mathrm{q_v}}(x,z,\eta,\tau)} \\ &= \overline{H_{\mathrm{q_v}}(x-u^\infty\tau,z,\eta-\int_0^\tau u^{(0)}(x,z,t')dt',0)} \\ &= \sigma(x-u^\infty\tau,z,0)\end{aligned} \tag{2.15}$$

It will turn out that the dynamics induced by the moisture in this model can all be tied to this σ. Looking at the definition (2.3) of the switching function $H_{\mathrm{q_v}}$ we see that

$$\begin{aligned}\sigma(x,z,\tau) &= \lim_{\eta_0\to\infty}\frac{1}{2\eta_0}\int_{-\eta_0}^{\eta_0} H_{\mathrm{q_v}}(x,z,\eta',\tau)d\eta' \\ &= \lim_{\eta_0\to\infty}\frac{|\{\eta\in(-\eta_0,\eta_0): q_{\mathrm{v}}(x,z,\eta,\tau)\geq q_{\mathrm{vs}}(z)\}|}{|(-\eta_0,\eta_0)|}\end{aligned} \tag{2.16}$$

So for a fixed point (x,z,τ), σ is the area fraction of saturated regions on the η-scale belonging to this point. Using (2.14) and the moist adiabatic equation

$$\theta_z^{(2)} = -\frac{\Gamma^{**}L^{**}q_{\mathrm{vs}}^{**}}{p^{(0)}}q_{\mathrm{vs},z}^{(0)} =: -\hat{L}q_{\mathrm{vs},z}^{(0)} \tag{2.17}$$

we can write (2.12) as

$$\hat{L}^{-1}\sigma\bar{w}^{(0)}\theta_z^{(2)} + \hat{L}^{-1}\overline{H_{q_{\mathrm{v}}}\tilde{w}^{(0)}}\theta_z^{(2)} = \overline{H_{q_{\mathrm{v}}}C_{\mathrm{d}}^{(0)}} \tag{2.18}$$

Now an expression for

$$w' := \overline{H_{q_{\mathrm{v}}}\tilde{w}^{(0)}} \tag{2.19}$$

is required. To obtain it, multiply both equations in (2.9) by $H_{q_{\mathrm{v}}}$ and average to get

$$\begin{aligned}w'_\tau + u^\infty w'_x &= \theta' \\ \theta'_\tau + u^\infty\theta'_x + w'\theta_z^{(2)} &= \hat{L}\left[(1-\sigma)\,\overline{H_{q_{\mathrm{v}}}C_{\mathrm{d}}^{(0)}} - \sigma\bar{C}_-\right]\end{aligned} \tag{2.20}$$

with

$$\theta' := \overline{H_{q_{\mathrm{v}}}\tilde{\theta}^{(3)}} \tag{2.21}$$

and, using (2.11) and $H_{q_{\mathrm{v}}}\left(H_{q_{\mathrm{v}}}-1\right)=0$,

$$\bar{C}_-(x,z,\tau) := \hat{L}C_{\mathrm{ev}}^{**}\overline{(H_{\mathrm{q_v}}-1)\left(q_{\mathrm{vs}}^{(0)}-q_{\mathrm{v}}^{(0)}\right)\sqrt{q_{\mathrm{r}}^{(0)}}} \tag{2.22}$$

From (2.10) and (2.11) one can see, that the leading order mixing ratio of rain, $q_{\mathrm{r}}^{(0)}$ is only advected with the flow for the chosen short timescale. The same holds for $q_{\mathrm{v}}^{(0)}$ so that the evaporation sourceterm $\bar{C}_-$ is also only advected and can thus be computed once in the beginning of a simulation and then just be moved around.

2.2. Summary of the model. The full model now consists of (2.8) with the $\bar{\theta}^{(3)}$ sourceterms replaced according to (2.18) and (2.22) plus (2.20) with the θ' sourceterm rewritten using (2.18). Summarized and dropping the superscripts 0 and 3 for simpler notation, this reads

$$\begin{aligned}
\bar{u}_\tau + u^\infty \bar{u}_x + \pi_x &= 0 \\
\bar{w}_\tau + u^\infty \bar{w}_x + \pi_z &= \bar{\theta} \\
\bar{\theta}_\tau + u^\infty \bar{\theta}_x + (1-\sigma)\,\theta_z^{(2)} \bar{w} &= \theta_z^{(2)} w' + \bar{C}_- \\
(\rho_0 \bar{u})_x + (\rho_0 \bar{w})_z &= 0 \\
w'_\tau + u^\infty w'_x &= \theta' \\
\theta'_\tau + u^\infty \theta'_x + \sigma \theta_z^{(2)} w' &= \sigma\,(1-\sigma)\,\theta_z^{(2)} \bar{w} - \sigma \bar{C}_-
\end{aligned} \tag{2.23}$$

Moisture effects the largescale dynamics given by the equations one to four in two ways. First, it reduces the effective stability of the atmosphere by a factor of $1-\sigma$, representing the effect that if a parcel rises and starts condensating water, the release of latent heat will effectively reduce the restoring force the parcel experiences. Because of the short timescale in this model, the only conversion mechanism between the moist quantities that has a leading order effect is the evaporation of cloudwater into vapor and the condensation of vapor into cloudwater in fully saturated regions and so σ itself does not change with time in the model.

Second, the release and consumption of latent heat by the averaged smallscale up- and downdrafts w' in saturated areas is described by the sourceterm $\theta_z^{(2)} w'$ in the equation for the largescale potential temperature plus the bulk microscale equations (equation five and six). A positive microscale vertical velocity w' results in a positive contribution to $\bar{\theta}$, modelling latent heat release while a negative w' models latent heat consumption.

For the scales used in the derivation, the effect that undersaturated regions in a rising parcel will eventually become saturated if it rises high enough is not present. An extension of the model to capture this effect will be a subject of future work, see the comments in 3.5.

The microscale model not only provides the sourceterm for the largescale dynamics but is also affected by them in return through the $\bar{w}$ sourceterm in the right hand side of the last equation. At last, for the chosen time- and lengthscales, the mass conservation equation reduces to the anelastic divergence constraint given by equation four, showing that acoustic waves have no significant effect in this regime.

Note that if all the moisture related terms vanish, i.e. $\sigma = 0$, $\bar{C}_- = 0$ and $w'(\tau = 0) = \theta'(\tau = 0) = 0$, (2.23) reduces to the linear, anelastic equations

$$\begin{aligned}
\bar{u}_\tau + u^\infty \bar{u}_x + \pi_x &= 0 \\
\bar{w}_\tau + u^\infty \bar{w}_x + \pi_z &= \bar{\theta} \\
\bar{\theta}_\tau + u^\infty \bar{\theta}_x + \theta_z^{(2)} \bar{w} &= 0 \\
(\rho_0 \bar{u})_x + (\rho_0 \bar{w})_z &= 0
\end{aligned} \tag{2.24}$$

See for example [4].

3. Properties of the model.

3.1. Dispersion relation. The asymptotic analysis yields, that the leading order density reads

$$\rho(z) = \exp(-z) \tag{3.1}$$

in nondimensional terms. Thus, the anelastic constraint in (2.23) can be rewritten as

$$\bar{u}_x + \bar{w}_z - \bar{w} = 0 \tag{3.2}$$

Applying a standard plane wave ansatz here would lead to a complex valued dispersion relation, as in an atmosphere with decreasing density the amplitude of gravity waves growth with height. To avoid this and obtain a real valued expression, we build this feature of growing amplitude into our ansatz. Plug

$$\phi(x, z, \tau) = \hat{\phi} \exp(\mu z) \exp(i(kx + mz - \omega\tau)) \tag{3.3}$$

with $\phi \in \{\bar{u}, \bar{w}, \bar{\theta}, \pi, w', \theta'\}$ into (2.23) and assume $\bar{C}_- = 0$, i.e. no source terms from evaporation and that σ is uniform in x. By successive elimination of the $\hat{\phi}$, we are left with roots

$$(\omega - u^\infty k)^2 = \omega_{\text{intr}}^2 = 0 \tag{3.4}$$

and

$$(\omega - u^\infty k)^2 = \frac{k^2 - \sigma(\mu^2 - \mu - m^2) - \sigma i(2\mu m - m)}{k^2 - (\mu^2 - \mu - m^2) - i(2\mu m - m)} \theta_z^{(2)} \tag{3.5}$$

The solution with $\omega_{\text{intr}} = 0$ corresponds to a vortical mode while the nonzero solutions are gravity waves. Choosing

$$\mu = \frac{1}{2} \tag{3.6}$$

results in the real valued dispersion relation

$$(\omega - u^\infty k)^2 = \frac{k^2 + \sigma(m^2 + \frac{1}{4})}{k^2 + m^2 + \frac{1}{4}} \theta_z^{(2)} \tag{3.7}$$

For $\sigma = 0$, this is equal to the dispersion relation for the pseudo-incompressible equation derived in [5]. Equation (3.7) can be rewritten as

$$\omega = u^\infty k + \omega_{\text{intr}} = u^\infty k \pm \sqrt{\frac{k^2 + \sigma(m^2 + \frac{1}{4})}{k^2 + m^2 + \frac{1}{4}} \theta_z^{(2)}} \tag{3.8}$$

Here, ω_{intr} is the so called intrinsic frequency, that would be seen by an observer moving with the background flow. Interestingly, for the incompressible case with $\rho_0 = const.$ in which the $1/4$ term vanishes, (3.8) is equal to the dispersion relation for internal gravity waves in a rotating fluid (see e.g. [11]), but with the Coriolis parameter f replaced by σ/N.

For the incompressible case, the dispersion relation can also be written as a function of the angle α between the direction of the wavevector (k, m) of a wave and the horizontal

$$\omega_{\text{intr}} = \sqrt{\left(\cos^2(\alpha) + \sigma \sin^2(\alpha)\right) \theta_z^{(2)}} \tag{3.9}$$

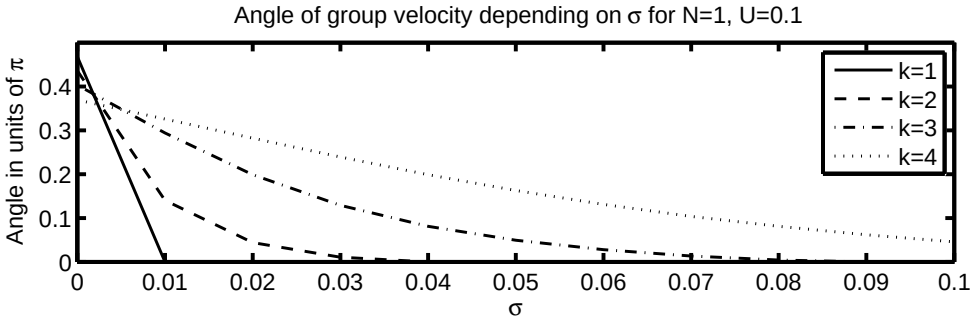

FIG. 3.1. *Angle between the direction of the group velocity and the horizontal for wavenumbers* $k = 1, \dots, 4$ *depending on* σ *in a steady state flow with* $N = 1$ *and* $U = 0.1$.

3.2. Group velocity. Taking the derivative of (3.8) with respect to k and m yields the group velocity of the waves

$$\mathbf{c}_{\mathrm{g}} = (u_{\mathrm{g}}, w_{\mathrm{g}}) = (u^{\infty}, 0) \pm \frac{(1-\sigma)\sqrt{\theta_z^{(2)}}}{(k^2+m^2+\frac{1}{4})^{\frac{3}{2}}(k^2+\sigma(m^2+\frac{1}{4}))^{\frac{1}{2}}} \left(k(m^2+\frac{1}{4}), -mk^2\right) \tag{3.10}$$

The group velocity is the velocity at which a packet of waves travels and it can be identified with the transportation of energy. In a dry ($\sigma = 0$), incompressible ($\mu = 0$, so no $\frac{1}{4}$ term) atmosphere, $\mathbf{c}_{\mathrm{g}}$ simplifies to the wellknown expression for the group velocity of internal waves in a stratified fluid (see e.g. [17]):

$$\mathbf{c}_{\mathrm{g,dry,inc}} = (u^{\infty}, 0) \pm \frac{m\sqrt{\theta_z^{(2)}}}{(k^2+m^2)^{\frac{3}{2}}} (m, -k) \tag{3.11}$$

One essential feature of these waves is that $\mathbf{c}_{\mathrm{g,dry,inc}} \perp (k, m)$, i.e. the direction in which these waves transport energy is perpendicular to their phase direction. Because of the 1/4 term, this no longer holds for (3.10), but still it can be seen that waves with upward directed phase (i. e. either positive m and positive branch in (3.8) and (3.10) or negative m and negative branch in (3.8) and (3.10)) have a downward directed group velocity and vice versa.

With increasing σ, the coefficient in (3.10) decreases and eventually, for $\sigma = 1$, becomes zero. Thus moisture reduces the transport of energy by waves and in fully saturated regions there is no energy transport by waves left at all, only advection of energy by the background flow u^{∞}.

The ratio of the vertical and horizontal component of the group velocity determines the slope at which a wave packet propagates

$$\Delta_{\mathrm{g}} = \frac{w_{\mathrm{g}}}{u_{\mathrm{g}}} \tag{3.12}$$

Figure 3.1 shows the angle between a line with slope $w_{\mathrm{g}}/u_{\mathrm{g}}$ and the horizontal depending on σ for a flow with $N = 1$ and $U = 0.1$. For all modes, moisture does decrease the angle of the group velocity, so we expect the angle at which a packet of mountain waves travel to become shallower with increasing σ. This is observed in the example in 4.1.2.

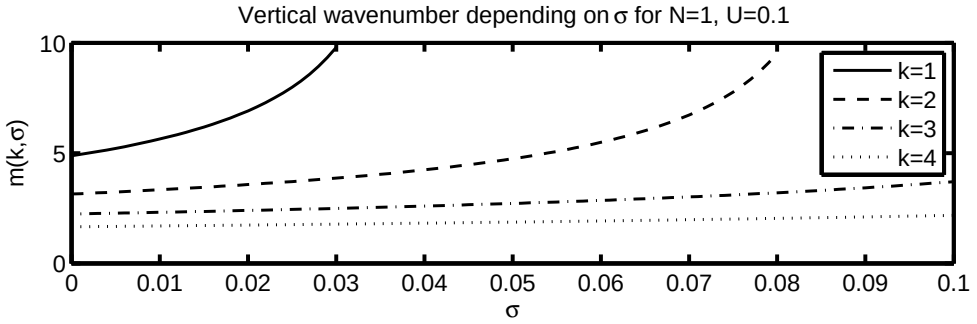

FIG. 3.2. *Vertical wavenumber m for $k = 1, \ldots, 4$ depending on σ.*

3.3. Taylor-Goldstein equation. A simplified but very illustrating class of solutions are those with a height dependent profile but a planewave structure in x and τ. We apply an ansatz

$$\phi(x, z, \tau) = \phi^{(k)}(z) \exp(\mu z) \exp(ik(x - c\tau)) \tag{3.13}$$

with $c = \omega/k$ being the horizontal phase speed observed at a fixed height z and $\phi \in \{\bar{u}, \bar{w}, \bar{\theta}, \pi, w', \theta'\}$. The additional term with parameter μ will, as in the derivation of the dispersion relation, describe the amplitude growth caused by the decreasing density in the anelastic model. Plugging this ansatz into (2.23) and eliminating all $\phi^{(k)}$ except for $\bar{w}^{(k)}$ yields

$$\left[\frac{\theta_z^{(2)} - k^2(u^\infty - c)^2}{k^2(u^\infty - c)^2 - \sigma\theta_z^{(2)}} k^2\right] \bar{w}^{(k)} + \mu(\mu - 1)\bar{w}^{(k)} + (2\mu - 1)\bar{w}_z^{(k)} + \bar{w}_{zz}^{(k)} = 0 \tag{3.14}$$

As in 3.1 we choose $\mu = 1/2$ here so that the final equation reads

$$\left[\frac{\theta_z^{(2)} - k^2(u^\infty - c)^2}{k^2(u^\infty - c)^2 - \sigma\theta_z^{(2)}} k^2 - \frac{1}{4}\right] \bar{w}^{(k)} + \bar{w}_{zz}^{(k)} = 0 \tag{3.15}$$

This equation is called Taylor-Goldstein equation and in the incompressible, dry case (i. e. with $\sigma = 0$ and without the $1/4$ term) it becomes the wellknown equation for internal gravity wave normal modes, see for example [10]. The coefficient in this equation is the square of the local vertical wavenumber, so

$$m(z, k) = \pm\sqrt{\left[\frac{\theta_z^{(2)} - k^2(u^\infty - c)^2}{k^2(u^\infty - c)^2 - \sigma\theta_z^{(2)}} k^2 - \frac{1}{4}\right]} \tag{3.16}$$

Figure 3.2 shows how the steady state vertical wavenumbers $m(k = 1, \ldots, 4)$ depend on σ for constant $\theta_z^{(2)}$ and u^∞. Obviously, moisture increases the vertical wavenumber.

Critical layers. Note that if there is a height z_c for which

$$c(z_c)^2 = (u^\infty)^2 - \sigma(z_c)\frac{\theta_z^{(2)}}{k^2} \tag{3.17}$$

then $m(z,k) \to \infty$ as $z \to z_c$ indicating a critical layer. In the dry case without shear, this can only happen if at some height the phase speed c is equal to the background velocity u^∞. In the moist case critical layers can also arise from the vertical profile of σ so that a noncritical dry flow can develop a critical layer if moisture is added. Also, the critical height z_c does depend on the horizontal wavenumber k in the moist case. A detailed investigation of the local structure of solutions in the presence of such critical layers will not be presented here but will be subject of future work.

3.4. Cutoff wavenumbers. For steadystate solutions it is $\omega_{\text{intr}} = 0$ and the dispersion relation (3.7) can be rewritten to express the vertical wavenumber m as a function of the horizontal wavenumber k only

$$m^2 = \frac{\theta_z^{(2)} - (u^\infty)^2 k^2}{(u^\infty)^2 k^2 - \sigma\theta_z^{(2)}} k^2 - \frac{1}{4} \tag{3.18}$$

We neglect the $1/4$ term as this simplifies the following derivation without qualitatively affecting the result. From (3.18) one can see, that for

$$k^2 > \frac{\theta_z^{(2)}}{(u^\infty)^2} \tag{3.19}$$

m becomes imaginary. Thus there is an upper limit up to which horizontal wavenumbers are actually propagated. Different from the dry case, moisture now also introduces a lower cutoff, as for

$$k^2 < \sigma \frac{\theta_z^{(2)}}{(u^\infty)^2} \tag{3.20}$$

m also becomes imaginary. So only horizontal wavenumbers k with

$$k_{\text{low}} := \sqrt{\sigma} \frac{\sqrt{\theta_z^{(2)}}}{u^\infty} \leq k \leq \frac{\sqrt{\theta_z^{(2)}}}{u^\infty} =: k_{\text{up}} \tag{3.21}$$

are propagating while waves with horizontal wavenumbers outside this range are evanescent. For increasing moisture, σ gets closer to one and the range of propagating wavenumbers narrows. In a completely saturated atmosphere with $\sigma = 1$, the only propagating mode left is $k = \sqrt{\theta^{(2)}}/u^\infty$.

A typical value for the stability frequency in dimensional terms is $N = 0.01 s^{-1}$ corresponding to $\sqrt{\theta_z^{(2)}} = 1$. Assume a typical backgroundflow of 10ms^{-1} (i.e. $u^\infty = 0.1$) and a not very moist atmosphere with $\sigma = 0.1$. Then the upper cutoff wavenumber is $k_{\text{up}} = 10$ and the lower is $k_{\text{low}} = \sqrt{\sigma}10 \approx 3.162$. Expressed in dimensional zonal wavelengths, this means that only wavelengths between roughly 6km and 20km propagate, while larger or smaller wavelengths are evanescent. The maximum wavelength decreases like $1/\sqrt{\sigma}$, so that small values of σ corresponding to small amounts of moisture can already filter a significant range of wavelengths: For $\sigma = 0.2$ the maximum wavelength is 14km and for $\sigma = 0.5$ the maximum wavelength is further reduced to about 8km.

3.5. Release of condensate. An important quantity is the amount of condensate that is released in a parcel of air due to condensation processes when the parcel is lifted. To assess it, the vertical displacement of a parcel from its initial position

has to be computed. Denote by $\xi(x,z,\tau)$ the vertical displacement of the air parcel at (x,z) at time τ. For a given verticel velocity field $\bar{w}$ it is

$$\frac{D\xi}{D\tau} = \xi_\tau(x,z,\tau) + u^\infty \xi_x(x,z,\tau) = \bar{w}(x,z,\tau) \tag{3.22}$$

so that ξ can be computed for a given $\bar{w}$ by solving (3.22).

Consider now a parcel that is at height z_0 at time $\tau = 0$. To this parcel belongs a η-scale distribution of watervapor, given by $q_\mathrm{v}(\eta,x,z,0)$. The air is saturated wherever $q_\mathrm{v}(\eta,x,z_0,\tau) \geq q_\mathrm{vs}(z_0)$ and condensation will take place if the parcel is displaced upward, so that the amount of watervapor in the parcel is reduced according to the decrease of saturation watervapor mixing ratio. Denote by $\delta q_\mathrm{v}(\xi;x,z_0)$ the condensate that the parcel initially located at (x,z_0) releases, if it is displaced upward from z_0 to $z_0+\xi$. For a parcel with $q_\mathrm{v}(\eta,x,z_0) \geq q_\mathrm{vs}(z_0)$ for every η, this amount can be approximated by

$$\delta q_\mathrm{v}(\xi;x,z_0) = q_\mathrm{vs}(z_0+\xi) - q_\mathrm{vs}(z_0) \approx \frac{dq_\mathrm{vs}(z_0)}{dz}\xi \tag{3.23}$$

If the parcel is not saturated everywhere, according to (2.16), $\sigma(x,z)$ is the area fraction of saturated areas and the condensate release can be approximated as

$$\delta q_\mathrm{v}(\xi;x,z_0) = q_\mathrm{vs}(z_0+\xi) - q_\mathrm{vs}(z_0) \approx \sigma(x,z)\frac{dq_\mathrm{vs}(z_0)}{dz}\xi \tag{3.24}$$

This approximation fails to account for the areas on the small scale which are initially undersaturated but reach saturation somewhere on the parcels ascend from z_0 to $z_0+\xi$, so that this definition of δq_v is more like a lower bound for the condensate release. However, as our linear model is only valid for small displacements anyhow, this will be a decent approximation for the actual condensate release except for peculiar distributions of $q_\mathrm{v}(\eta)$ with large undersaturated regions that are very close to saturation. Note that (3.24) holds for positive displacements ξ, a parcel that is displaced downward by a negative ξ does not release condensate.

There is also an interesting possible extension of the model emerging from this derivation: If one assumes that the air is saturated at leading order, i.e. $q_\mathrm{vs}^{(0)} = q_\mathrm{v}^{(0)}$ everywhere and then defines σ according to the first order watervapor distribution $q_\mathrm{v}^{(1)}$, σ is no longer only advected by the background flow. Instead the equation for σ then also contains the vertical velocity $\bar{w}$, making this modified model nonlinear. The discussion of this extension is subject of future work.

4. Numerical results. To solve the system (2.23) numerically, a projection method is used. The predictor step is solved by a third order Adams-Bashforth scheme in time together with a fourth order central difference scheme for the advective terms. The application of this scheme to advection problems was investigated in [6] and found to be a viable alternative to the commonly used leapfrog scheme. Then a projection is performed, computing a pressure field that ensures that the velocity satisfies the anelastic constraint. To solve the Laplace problem occuring in the projection step, we use the discretization described in [19] with slight modifications to account for the varying density ρ_0. Details of the discretization can be found in the appendix.

4.1. Steady state solutions for a uniform atmosphere. If $\theta_z^{(2)}$, σ and u^∞ are constant and periodic boundary conditions are assumed in horizontal direction,

analytical solutions of the form

$$\bar{w}(x,z) = \exp(\frac{1}{2}z) \sum_{n=-N_x}^{n=N_x} \hat{\bar{w}}^{(n)}(z) \exp(ik_n x) \tag{4.1}$$

with $k_n = \frac{2\pi n}{l}$, l equal to the length of the domain can be derived, whereas every $w^{(n)}$ is a solution of (3.15) with $k = k_n$. If all coefficients are constant, these solutions simply read

$$\hat{\bar{w}}^{(k_n)} = A^{(k_n)} \exp(im(k_n)z) + B^{(k_n)} \exp(-im(k_n)z) \tag{4.2}$$

To avoid energy propagating downward, i.e. a negative vertical component of $\mathbf{c}_\mathrm{g}$, we choose the negative branch in (3.16) and set $B^{(k_n)} = 0$. The coefficient $A^{(k_n)}$ is determined according to the lower boundary condition

$$\bar{w}(x, z = 0, t) = u^\infty h_x(x) \tag{4.3}$$

where h describes the topography.

4.1.1. Sine shaped topography. At first, we illustrate the change of the vertical wavenumber as well as the lower cutoff for the case of a simple, sine shaped topography

$$h(x) = H \sin(2x) \tag{4.4}$$

on a domain $[0, 2\pi] \times [0, 1]$ that will only excite a single mode with horizontal wavenumber $k = 2$. Values for σ are $\sigma = 0$, $\sigma = 0.02$ and $\sigma = 0.05$. The stratification is $\sqrt{\theta_z^{(2)}} = 1$ and the backgroundflow $u^\infty = 0.1$, so the lower cutoff wavenumbers are $k_\mathrm{low} = \sqrt{0.02} \cdot (1/0.1) \approx 1.41$ and $k_\mathrm{low} = \sqrt{0.05} \cdot (1/0.1) \approx 2.24$ respectively. The height of the topography is set to $H = 0.04$, corresponding to a dimensional value of 400m. Figure 4.1 shows contour lines of the vertical velocity $\bar{w}$ for the three different values of σ. The first figure shows the dry solution. In the second figure with $\sigma = 0.02$ it is still $k_\mathrm{low} < k$ so the wave excited by the hill is propagating. Compared to the dry case, the direction of propagation is slightly tilted to the vertical, corresponding to the increase of the vertical wavenumber $m(k)$ with increasing σ. In the third figure with $\sigma = 0.05$, the solution has completely changed. Now it is $k < k_\mathrm{low}$ so the excited wave does no longer propagate but is now evanescent and its amplitude decays exponentially with height. Only a very small response can be seen in the lower part of the domain.

4.1.2. Witch of Agnesi. A more complex case is the so called Witch of Agnesi topography which excites modes of all wavenumbers k:

$$h(x) = \frac{HL^2}{L^2 + (x - x_\mathrm{c})^2} \tag{4.5}$$

Here, H is the height of the hill, L is a measure of its length and x_c is the center of the domain, so that the top of the hill is in the middle of it. Figure 4.2 shows solutions with $N_x = 201$ for $\sigma = 0$, $\sigma = 0.1$ and $\sigma = 0.5$ for $\sqrt{\theta_z^{(2)}} = 1$, $u^\infty = 0.1$. The computational domain is $[0, 8] \times [0, 1]$ but the solution is plotted only on $[2, 6] \times [0, 1]$. The hill has a height of $H = 0.04$ and a length of $L = 0.1$.

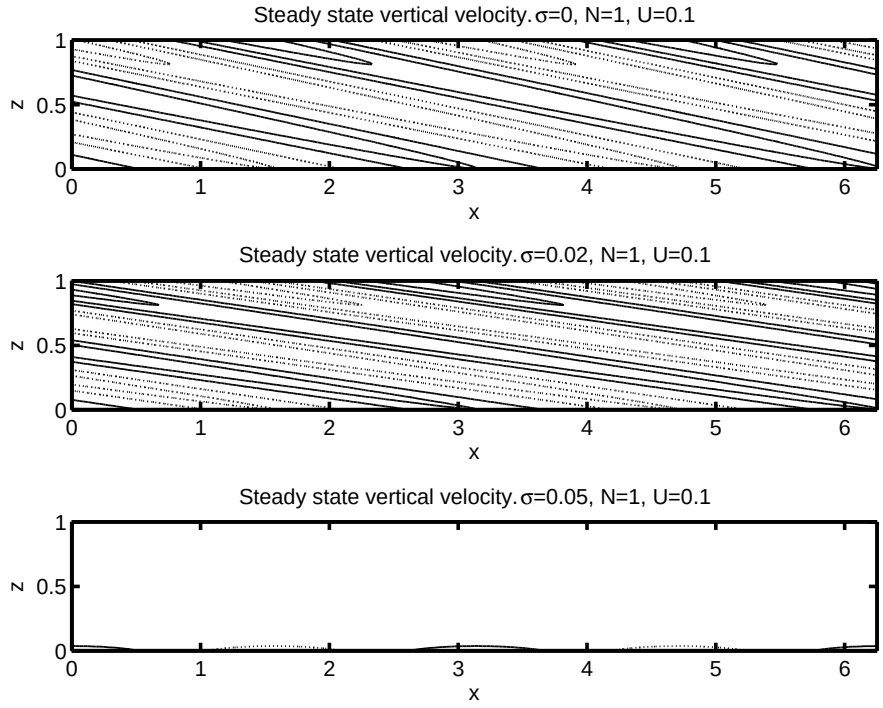

FIG. 4.1. *Contourlines of the steady state vertical velocity for a sine shaped topography with horizontal wavenumber $k = 2$ for $\sigma = 0$, $\sigma = 0.02$ and $\sigma = 0.05$. The intervall between contours is 0.02 or $0.2m/s$ in dimensional terms. Dotted contours represent negative values.*

With increasing σ, the slope of the wave pattern is reduced, according the the reduced slope of the group velocity pointed out in 3.2. The dashed lines visualize the average over the slopes (3.12) of all propagating modes, where each mode is weighted by its amplitude. The reduction of the angle of propagation is compatible with the following consideration: As moisture does decrease the stability N of the atmosphere, it does also decrease the nondimensional parameter

$$\frac{NL}{u^\infty} \tag{4.6}$$

which is a large for waves close to hydrostatic balance. As hydrostatic waves propagate only in the vertical and the horizontal component does increase as waves become more nonhydrostatic, it seems reasonable that a reduction of (4.6) by moisture leads to a reduction of the propagation angle.

As σ increases and more and more modes turn into evanescent, the amplitude of the wave pattern is reduced.

An important mechanism caused by gravity waves is the vertical transfer of horizontal momentum. While for propagating modes the horizontally averaged vertical flux of momentum $\overline{\rho^{(0)}\bar{u}\bar{w}}$ is constant [1], for evanescent modes it also decays exponentially with height. Thus by turning propagating modes into evanescent modes, moisture in this model inhibits the momentum transfer by gravity waves. Tabular 4.1

[1] For once here, the overbar denotes the horizontal average in x and not in η.

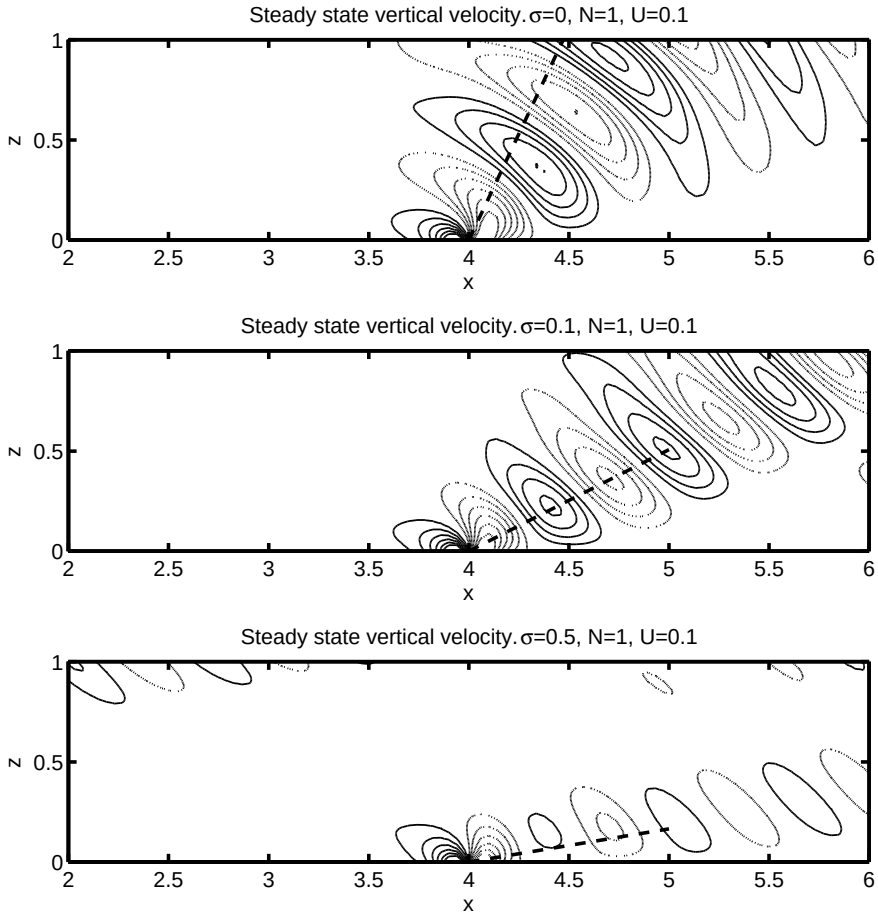

FIG. 4.2. *Contourlines of the steady state vertical velocity for a Witch of Agnesi topography with* $H = 0.04$ *and* $L = 0.1$ *for* $\sigma = 0$, $\sigma = 0.1$ *and* $\sigma = 0.5$. *The intervall between contours is* 0.025 *or* $0.25m/s$ *in dimensional terms. Dotted contours represent negative values. The dashed lines visualize the averaged slope of the group velocity of all propagating modes.*

TABLE 4.1
Vertical flux of horizontal momentum for different values of σ *in the constant coefficient, steady state solution.*

σ	*nondimensional momentum flux*
0	$-5.68 \cdot 10^{-3}$
0.1	$-4.81 \cdot 10^{-3}$
0.5	$-1.73 \cdot 10^{-3}$

lists the values of the horizontally averaged vertical flux of momentum at the top of the domain for different values of σ.

4.2. Mountain waves disturbed by a moving cloud. In this subsection, we want to demonstrate the effects of a cloud being advected through an established mountain wave pattern, so the fully timedependent problem (2.23) is now solved numerically. The domain is $[-2, 2] \times [0, 1.5]$. To realize a transparent upper boundary

condition, a Rayleigh damping layer as described in [16] reaching from $z = 1$ to $z = 1.5$ is used. The topography is a Witch-of-Agnesi hill as in 4.1.2 with $H = 0.04$ and $L = 0.1$ and the maximum located at $x = 0$ here. The background flow is linearly increased from $\tau = 0$ to $\tau = 0.25$ up to its maximum value of $u^\infty = 0.1$.

The simulation is run until $\tau_\sigma = 3$ with $\sigma \equiv 0$. Then, a cloud described by a Gaussian distributed σ is introduced which is subsequently advected with velocity u^∞, crosses the domain and finally exits at the right boundary. For $\tau \geq \tau_\sigma$ it is

$$\sigma(x, z, \tau) = \sigma_{\max} \exp\left(-\frac{1}{2}\left[\frac{(x - x_c - u^\infty[\tau - \tau_\sigma])^2}{s_x^2} + \frac{(z - z_c)^2}{s_z^2}\right]\right) \tag{4.7}$$

with $\sigma_{\max} = 0.5$, $s_x = 1$, $s_z = 0.05$ and $z_c = 0.4$. To avoid a sudden introduction of moisture into the model at $\tau = \tau_\sigma$, we set

$$x_c = x_{\text{left}} - 2 \cdot s_x \quad \text{with} \quad x_{\text{left}} = -2 \tag{4.8}$$

so that at τ_σ the maximum of σ is far outside the actual domain of computation at $x = -4$. The cloud is then advected with velocity $u^\infty = 0.1$ into the domain so that its maximum enters at $\tau = \tau_\sigma + \frac{x_c}{u^\infty} = 20$ at the left boundary and leaves the domain at $\tau = \tau_\sigma + \frac{x_c}{u^\infty} + \frac{4}{u^\infty} = 60$. The maximum is always located at a height of $z = 0.4$.

The simulation used 200 nodes in horizontal direction and 75 in the vertical, resulting in a horizontal and vertical resolution of $\Delta x = \Delta z = 0.02$ or 200m. The timestep is $\Delta\tau = 0.05$ or 5s.

The first four figures in 4.3 shows contourlines of the vertical velocity $\bar{w}$ at different times. At $\tau = 27.5$ in the first figure, the cloud has entered the domain from the left. Inside the cloud, some small up- and downdrafts exist, generated by the amplification through latent heat release or consumption. Figures two, three and four show how the clouds travels through the mountain waves. For comparison, the last figure shows a dry reference solution also at $\tau = 50$. Comparing figure four and five, one can cleary see how the cloud has damped the waves above it as well as how inside the cloud existing up- and downdrafts are amplified, generating a sequence of new extrema of vertical velocity.

4.3. Waves travelling through clouds. The domain is $[0, 20] \times [0, 1]$ and there is no backgroundflow here, i.e. $u^\infty = 0$. In this example the stability frequency is $\sqrt{\theta_z^{(2)}} = 2.5$. Between $x = 4$ and $x = 6$ and $x = 14$ and $x = 16$, two clouds are located with their maximum at $z = 0.5$.

All initial values are zero, except for a concentrated gaussian peak of negative $\bar{\theta}$, placed in the center of the domain with its maximum at $(x, z) = (10, 0.5)$. Figure 4.4 visualizes both the distribution of σ as well as the initial $\bar{\theta}$. The simulation used 200 nodes in horizontal direction, 40 nodes between $z = 0$ and $z = 1$ plus 10 more nodes to realize the sponge layer above $z = 1$. The timestep is $\Delta\tau = 0.1$. For comparison, a reference solution is computed with identical parameters but $\sigma \equiv 0$ everywhere.

The initial potential temperature perturbation starts to excite waves, which form a typical X-shaped pattern (not shown). Figure 4.5 shows a crosssection through the vertical velocity at $z = 0.5$ of the cloudy case (continous line) as well as the noncloudy reference simulation (dashed line). In the first figure at $\tau = 5$, waves have formed and started travelling outwards. Inside the cloud, the updraft due to the entering wave is amplified by latent heat release. As the wave is also slowed inside the cloud, there is some steepening of the wave at the beginning of the cloud. In the next figure at $\tau = 7$, the steepening before the cloud as well as the amplification inside it are

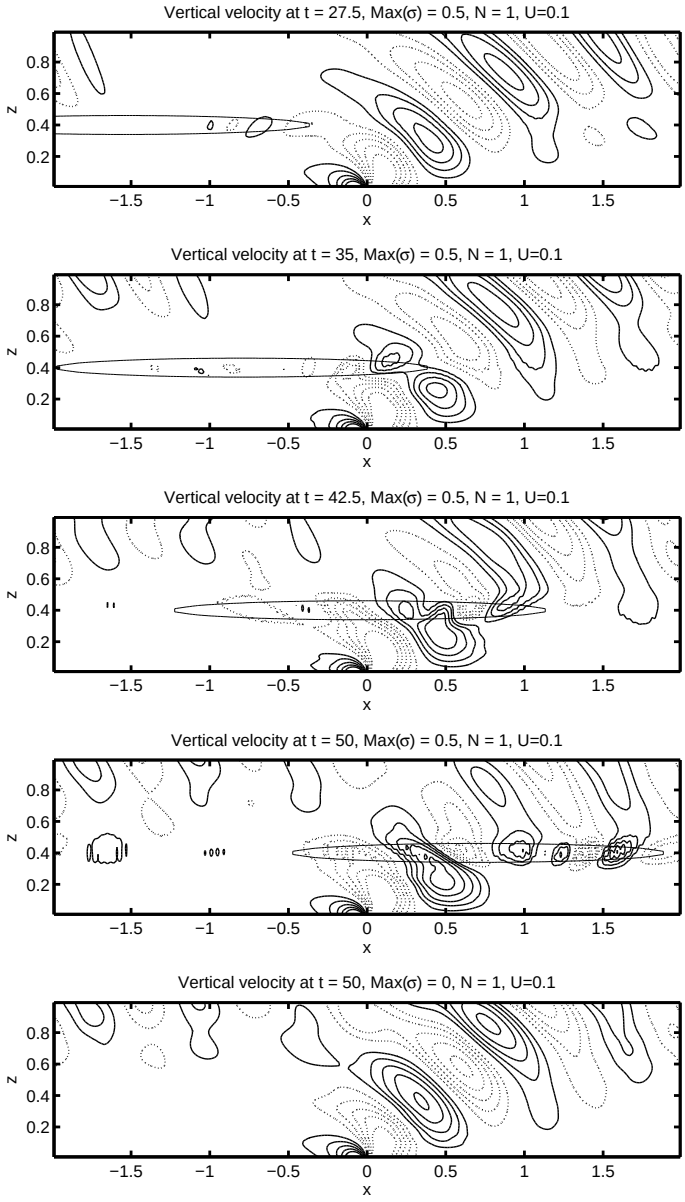

FIG. 4.3. *Contourlines of the vertical velocity at different times for a cloud being advected through the waves excited by a Witch of Agnesi. Intervall between contours is* 0.025 *or* $0.25m/s$ *in dimensional terms. Dotted contours represent negative values. The thin, ellipse shaped contour is the* $\sigma = 0.25$ *contourline. The last figure shows a reference solution without any moisture at* $\tau = 50$ *for comparison.*

even more pronounced. In the last figure at $\tau = 14$ one can see the newly formed extrema and a generally strongly distorted distribution of vertical velocity inside the cloud. However, in the region far behind the cloud, the wave is clearly damped when compared to the noncloudy case.

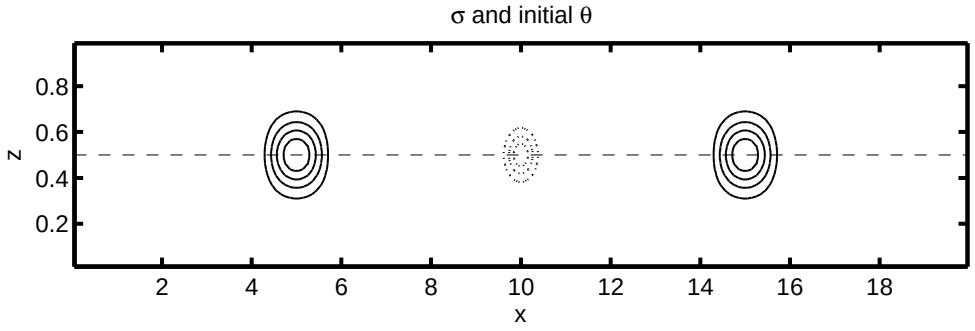

FIG. 4.4. *σ modelling two clouds. The dashed line is the crosssection along which the vertical velocity is plotted in figure 4.5. The continous lines are isolines of σ with a difference between isolines of* 0.1 *and the outer isoline corresponding to $\sigma = 0.1$. The dotted line shows the initial distribution of $\bar{\theta}$, the difference between the isolines is* 0.025*, the outer line corresponding to $\bar{\theta} = -0.025$.*

5. Conclusions. Starting from the results in [15], we derived a model for the interaction of internal gravity waves with a timescale of 100s and a lengthscale of 10km and convective hot towers which vary on a horizontal 1km scale. The closing of the model was achieved by the application of weighted averages over the small 1km horizontal scale and did not require additional approximations. It turned out, that the effects of moisture in the model are all related to a parameter σ which describes the area fraction of saturated patches on the small scale.

The resulting equations were an extension of the linear, anelastic model. Moisture did reduce the effective stability in the model and provided a condensation / evaporation sourceterm for potential temperature, defined by two additional equations for weighted averages of the small scale perturbations of potential temperature and vertical velocity. However, the equations for these small scale perturbations not only provided the sourceterm for the largescale potential temperature but are themselves affected by the largescale flow, so that the model sees an interaction between small and largescale quantities.

The dispersion relation and group velocity of this extended model was computed. It was found that moisture, occuring as the beforementioned σ in the model, does introduce a lower cutoff horizontal wavenumber, turning modes below this threshold from propagating into evanescent. This effect was demonstrated by showing steadystate solutions excited by a sine shaped topography. It was also noted, that moisture can cause critical layers for flows that would be noncritical in dry conditions.

Examination of the group velocity showed that moisture does decrease the energy transport by waves, shutting it down completely if the atmosphere is fully saturated, i.e. $\sigma = 1$. Also, while moisture was found to increase the vertical wavenumber of each individual mode, it was also found to reduce the slope of the group velocity, so that the angle of propagation of a wave package is reduced. As an example, the steadystate solutions for mountain waves excited from a Witch of Agnesi topography for different values of σ were shown.

Two examples of numerically computed, fully timedependent solutions were given. First, a cloud represented as a Gaussian distributed σ was advected through the mountain waves excited by a Witch of Agnesi topography. A significant damping of the waves above the cloud could be seen as well as the generation of new extrema of vertical velocity inside the cloud. The second example placed a small perturbation

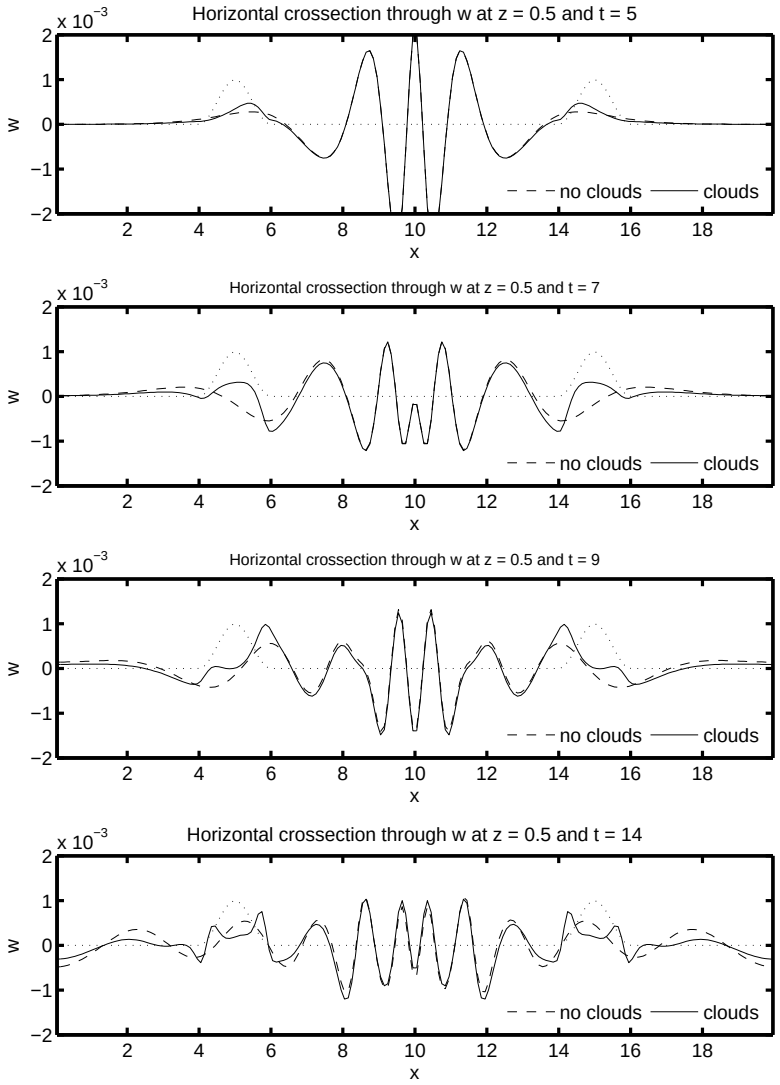

FIG. 4.5. *Cross section of the vertical velocity $\bar{w}$ at different times for the cloudy and noncloudy case. The dotted line is the crosssection through σ at the same height, but scaled down by a factor of* 0.002 *so that the shape is reasonably visible in the given scaling of the y-axis.*

of potential temperature between two clouds, so that the waves excited from the perturbation travel through them. The amplification of up- and downdrafts inside the cloud as well as the damping of the waves in the region behind the clouds was observed.

Acknowledgments. This research is partially funded by Deutsche Forschungsgemeinschaft, MetStroem SPP 1276 and PQP SSP 1167.

REFERENCES

[1] A. Barcilon and D. Fitzjarrald, *A nonlinear steady model for moist hydrostatic mountain waves*, J. Atmosph. Sci., 42 (1985), pp. 58–67.
[2] A. Barcilon, J. C. Jusem, and S. Blumsack, *Pseudo-adiabatic flow over a two-dimensional ridge*, Geophys. Astrophys. Fluid Dynamics, 16 (1980), pp. 19–33.
[3] A. Barcilon, J. C. Jusem, and P. G. Drazin, *On the two-dimensional, hydrostatic flow of a stream of moist air over a mountain ridge*, Geophys. Astrophys. Fluid Dynamics, 13 (1979), pp. 125–140.
[4] T. Davies, A. Staniforth, N. Wood, and J. Thuburn, *Validity of anelastic and other equation sets as inferred from normal-mode analysis*, Q. J. R. Meteorol. Soc., 129 (2003), pp. 2761–2775.
[5] D. R. Durran, *Improving the anelastic approximation*, J. Atmosph. Sci, 46 (1989), pp. 1453–1461.
[6] D. R. Durran, *The third-order adams-bashforth method: An attractive alternative to leapfrog time differencing*, Mon. Wea. Rev., 119 (1991), pp. 702–720.
[7] D. R. Durran and J. B. Klemp, *A compressible model for the simulation of moist mountain waves*, Mon. Wea. Rev., 111 (1983), pp. 2341–2361.
[8] F. Einaudi and D. P. Lalas, *The propagation of acoustic-gravity waves in a moist atmosphere*, J. Atmosph. Sci., 30 (1973), pp. 365–376.
[9] K. A. Emanuel, *Atmospheric Convection*, Oxford University Press, 1994.
[10] D. Etling, *Theoretische Meteorologie*, Springer, 1996.
[11] A. E. Gill, *Atmosphere-Ocean Dynamics*, Academic Press, 1982.
[12] W. W. Grabowski, *Toward cloud resolving modeling of large-scale tropical circulations: A simple cloud microphysics parameterization*, J. Atmosph. Sci., 55 (1998), pp. 3283–3298.
[13] J. C. Jusem and A. Barcilon, *Simulation of moist mountain waves with an anelastic model*, Geophys. Astrophys. Fluid Dynamics, 33 (1985), pp. 259–276.
[14] R. Klein, *An applied mathematical view of meteorological modelling*, in Applied Mathematics Entering the 21st century; Invited talks from the ICIAM 2003 Congress, vol. 116, SIAM Proceedings in Applied Mathematics, 2004.
[15] R. Klein and A. Majda, *Systematic multiscale models for deep convection on mesoscales*, Theor. & Comput. Fluid Dyn., 20 (2006), pp. 525–551.
[16] J. B. Klemp and D. K. Lilly, *Numerical simulation of hydrostatic mountain waves*, J. Atmosph. Sci., 35 (1978), pp. 78–107.
[17] J. Lighthill, *Waves in Fluids*, Cambridge University Press, 1978.
[18] A. J. Majda, *Multiscale models with moisture and systematic strategies for superparameterization*, J. Atmosph. Sci., 64 (2007), pp. 2726–2734.
[19] S. Vater, *A new projection method for the zero froude number shallow water equations*. PIK Report No. 97, 2005.

Appendix A. Vertical velocity, potential temperature, pressure and density are expanded as described in [15], but are now also allowed to depend on the new, fast timescale τ':

$$\begin{aligned} w(x,z,t;\epsilon) &= w^{(0)}(\eta,x,z,\tau,\tau') + \mathcal{O}(\epsilon) \\ \theta(x,z,t;\epsilon) &= 1 + \epsilon^2\theta^{(2)}(z) + \epsilon^3\theta^{(3)}(\eta,x,z,\tau,\tau') + \mathcal{O}(\epsilon^4) \\ (p,\rho)(x,z,t;\epsilon) &= (p^{(0)},\rho^{(0)})(z) + \epsilon(p^{(1)},\rho^{(1)})(z) + \epsilon^2(p^{(2)},\rho^{(2)})(z) \\ &\quad +\epsilon(p^{(3)},\rho^{(3)})(\eta,x,z,\tau,\tau') + \mathcal{O}(\epsilon^4) \end{aligned} \tag{A.1}$$

The mixing ratios for watervapor, cloudwater and rainwater are expanded as

$$(q_\mathrm{v},q_\mathrm{c},q_\mathrm{r}) = \left(q_\mathrm{v}^{(0)},q_\mathrm{c}^{(0)},q_\mathrm{r}^{(0)}\right)(\eta,x,z,\tau,\tau') + \epsilon\left(q_\mathrm{v}^{(1)},q_\mathrm{c}^{(1)},q_\mathrm{r}^{(1)}\right)(\eta,x,z,\tau,\tau') + \mathcal{O}(\epsilon^2) \tag{A.2}$$

The bulk moisture equations for the mixing ratio of watervapor, cloudwater and rainwater read

$$\begin{aligned} q_{v,t} + \mathbf{u}\cdot\nabla_{||} q_v + w q_{v,z} &= -\epsilon^{-n}\hat{C}_{\mathrm{d}} + \hat{C}_{\mathrm{ev}} \\ q_{c,t} + \mathbf{u}\cdot\nabla_{||} q_c + w q_{c,z} &= \epsilon^{-n}\hat{C}_{\mathrm{d}} - \epsilon^{-1}\hat{C}_{\mathrm{cr}} - \hat{C}_{\mathrm{ac}} \\ q_{r,t} + \mathbf{u}\cdot\nabla_{||} q_r + w q_{r,z} + \rho^{-1}\left(V_{\mathrm{T}}^{**}\rho q_r\right)_z &= \epsilon^{-1}\hat{C}_{\mathrm{cr}} - \hat{C}_{\mathrm{ev}} + \hat{C}_{\mathrm{ac}} \end{aligned} \tag{A.3}$$

The sourceterms on the righthand side represent condensation, evaporation, collection of cloudwater by falling rain and autoconversion of cloudwater to precipitation.

Appendix B. The nondimensional conservation laws for mass, momentum, energy (expressed as potential temperature) in [15] read

$$\begin{aligned} \rho_t + \nabla_{||}\cdot(\rho\mathbf{u}) + (\rho w)_z &= 0 \\ \mathbf{u}_t + \mathbf{u}\cdot\nabla_{||}\mathbf{u} + w\mathbf{u}_z + \epsilon f\left(\Omega\times\mathbf{v}\right)_{||} + \epsilon^{-4}\rho^{-1}\nabla_{||}p &= 0 \\ w_t + \mathbf{u}\cdot\nabla_{||} w + w w_z + \epsilon f\left(\Omega\times\mathbf{v}\right)_{\perp} + \epsilon^{-4}\rho^{-1}p_z &= -\epsilon^{-4} \\ \theta_t + \mathbf{u}\cdot\nabla_{||}\theta + w\theta_z &= \epsilon^2\left(\tilde{S}_\theta^\epsilon + S_\theta^{q,\epsilon}\right) \end{aligned} \tag{B.1}$$

where

$$S_\theta^{q,\epsilon} = \Gamma^{**}L^{**}q_{\mathrm{vs}}^{**}\frac{\theta}{p}\left(\epsilon^{-n}\hat{C}_{\mathrm{d}} - \hat{C}_{\mathrm{ev}}\right) \tag{B.2}$$

is the sourceterm related to evaporation and condensation while $\tilde{S}_\theta^\epsilon$ is a given external source of energy like, for example, radiation. The doublestar quantities are constant scaling factors that have been introduced in the nondimensionalisation. Inserting (2.5), (A.1) and (A.2) into (B.1) and (A.3) yields the following leading order equations

Horizontal momentum.

$$\begin{aligned} \mathcal{O}(\epsilon^2) &: \; p_\eta^{(3)} = 0 \\ \mathcal{O}(\epsilon^3) &: \; \rho^{(0)}u_\tau^{(0)} + \rho^{(0)}u_{\tau'}^{(1)} + \rho^{(0)}u^\infty u_x^{(0)} + \rho^{(0)}u^\infty u_\eta^{(1)} \\ &\quad + p_x^{(3)} + p_\eta^{(4)} = 0 \end{aligned} \tag{B.3}$$

The second equation can be rewritten as

$$\rho^{(0)}u_\tau^{(0)} + \rho^{(0)}u^\infty u_x^{(0)} + p_x^{(3)} = -\left[\rho^{(0)}u_{\tau'}^{(1)} + \rho^{(0)}u^\infty u_\eta^{(1)} + p_\eta^{(4)}\right] \tag{B.4}$$

By integrating this equation along a characteristic $\tau' + u^\infty\eta = const.$ and employing sublinear growth condition for the higher order quantities $u^{(1)}$ and $p^{(4)}$, we conclude that the right hand side must be zero and the equation simplifies to

$$\rho^{(0)}u_\tau^{(0)} + \rho^{(0)}u^\infty u_x^{(0)} + p_x^{(3)} = 0 \tag{B.5}$$

Note that as u^∞ was assumed to be constant, there is no term $w^{(0)}u_z^\infty$ occuring here.

Vertical momentum.

$$\begin{aligned}
\mathcal{O}(1) &: p_z^{(0)} = -\rho^{(0)} \\
\mathcal{O}(\epsilon) &: p_z^{(1)} = -\rho^{(1)} \\
\mathcal{O}(\epsilon^2) &: \rho^{(0)} w_{\tau'}^{(0)} + \rho^{(0)} u^\infty w_\eta^{(0)} + p_z^{(2)} = -\rho^{(2)} \\
\mathcal{O}(\epsilon^3) &: \rho^{(0)} w_{\tau'}^{(1)} + \rho^{(0)} u^\infty w_\eta^{(1)} + \rho^{(1)} w_{\tau'}^{(0)} + \rho^{(1)} u^\infty w_\eta^{(0)} \\
&\quad + \rho^{(0)} w_\tau^{(0)} + \rho^{(0)} u^\infty w_x^{(0)} + \rho^{(0)} u^{(0)} w_\eta^{(0)} + p_z^{(3)} = -\rho^{(3)}
\end{aligned} \tag{B.6}$$

We assume $\rho^{(1)} = 0$ here and employ again the sublinear growth condition. The last equation then becomes

$$\rho^{(0)} w_\tau^{(0)} + \rho^{(0)} u^\infty w_x^{(0)} + \rho^{(0)} u^{(0)} w_\eta^{(0)} + p_z^{(3)} = -\rho^{(3)} \tag{B.7}$$

Under the assumption that the specific heats c_v and c_p are constants and by employing the Newtonian limit, expanding the equation of state yields

$$-\frac{\rho^{(3)}}{\rho^{(0)}} = \theta^{(3)} - \frac{p^{(3)}}{p^{(0)}} \tag{B.8}$$

Using this and the hydrostatic balance for the leading order density and pressure, one obtains

$$w_\tau^{(0)} + u^\infty w_x^{(0)} + u^{(0)} w_\eta^{(0)} \pi_z^{(3)} = \theta^{(3)} \tag{B.9}$$

with $\pi^{(3)} := p^{(3)}/\rho^{(0)}$.

Mass.

$$\rho^{(0)} u_\eta^{(1)} + \rho^{(0)} u_x^{(0)} + \left(\rho^{(0)} w^{(0)}\right)_z = 0 \tag{B.10}$$

Sublinear growth yields

$$\rho^{(0)} u_x^{(0)} + \left(\rho^{(0)} w^{(0)}\right)_z = 0 \tag{B.11}$$

Potential temperature.

$$\begin{aligned}
\mathcal{O}(\epsilon^3) &: \theta_{\tau'}^{(3)} + u^\infty \theta_\eta^{(3)} = 0 \\
\mathcal{O}(\epsilon^4) &: \theta_\tau^{(3)} + \theta_{\tau'}^{(4)} + u^\infty \theta_x^{(3)} + u^\infty \theta_\eta^{(4)} + u^{(0)} \theta_\eta^{(3)} + w^{(0)} \theta_z^{(2)} \\
&\quad = \frac{L^{**}\Gamma^{**} q_\mathrm{vs}^{**}}{p_0} \left(H_{\mathrm{q_v}} C_\mathrm{d}^{(0)} + (H_{\mathrm{q_v}} - 1) C_\mathrm{ev}^{(0)} \right)
\end{aligned} \tag{B.12}$$

assuming that there are no external sources of heat, i.e. $\tilde{S}_\theta^\epsilon = 0$. Again, the advective derivative of $\theta^{(4)}$ along $\tau' - \eta$ characteristics is eliminated by the sublinear growth condition:

$$\theta_\tau^{(3)} + u^\infty \theta_x^{(3)} + u^{(0)} \theta_\eta^{(3)} + w^{(0)} \theta_z^{(2)} = \frac{L^{**}\Gamma^{**} q_\mathrm{vs}^{**}}{p_0} \left(H_{\mathrm{q_v}} C_\mathrm{d}^{(0)} + (H_{\mathrm{q_v}} - 1) C_\mathrm{ev}^{(0)} \right) \tag{B.13}$$

Note that if $u^\infty = 0$ (B.3) to (B.12) reduce to the equations (76) to (80) in [15].

From the equation for the transport of watervapor we get

$$\begin{aligned}
\mathcal{O}(\epsilon^{-n}) &: C_{\mathrm{d}}^{(-n)} \sim C_{\mathrm{d}}^{**}\delta q_{\mathrm{vs}}^{(0)} H_{\circ} q_{\mathrm{c}}^{(0)} = 0 \\
\mathcal{O}(\epsilon^{-n+1}) &: C_{\mathrm{d}}^{(-n+1)} \sim C_{\mathrm{d}}^{**}\delta q_{\mathrm{vs}}^{(1)} H_{\circ} q_{\mathrm{c}}^{(0)} = 0 \\
\mathcal{O}(\epsilon^{-n+2}) &: C_{\mathrm{d}}^{(-n+2)} \sim C_{\mathrm{d}}^{**}\delta q_{\mathrm{vs}}^{(2)} H_{\circ} q_{\mathrm{c}}^{(0)} = 0
\end{aligned} \tag{B.14}$$

so that we can distinguish the regimes of nearly saturated air with where the saturation deficit δq_{vs} is nonzero only at high orders and the undersaturated regime in which $q_{\mathrm{c}}^{(0)} = 0$, i.e. the cloudwater mixing ratio is zero at leading order. The equations for the two regimes are:

Saturated air.

$$\begin{aligned}
&q_{\mathrm{vs},\tau'}^{(2)} + u^{\infty} q_{\mathrm{vs},\eta}^{(2)} + w^{(0)} q_{\mathrm{vs,z}}^{(0)} = -C_{\mathrm{d}}^{(0)} \\
&q_{\mathrm{c},\tau'}^{(1)} + u^{\infty} q_{\mathrm{c},\eta}^{(1)} = 0 \\
&q_{\mathrm{c},\tau'}^{(2)} + u^{\infty} q_{\mathrm{c},\eta}^{(2)} + q_{\mathrm{c},\tau}^{(1)} + u^{\infty} q_{\mathrm{c,x}}^{(1)} + u^{(0)} q_{\mathrm{c},\eta}^{(1)} = C_{\mathrm{d}}^{(0)} - C_{\mathrm{cr}}^{(0)} \\
&q_{\mathrm{r},\tau'}^{(0)} + u^{\infty} q_{\mathrm{r},\eta}^{(0)} = 0 \\
&q_{\mathrm{r},\tau'}^{(1)} + u^{\infty} q_{\mathrm{r},\eta}^{(1)} + q_{\mathrm{r},\tau}^{(0)} + u^{\infty} q_{\mathrm{r,x}}^{(0)} + u^{(0)} q_{\mathrm{r},\eta}^{(0)} = 0
\end{aligned} \tag{B.15}$$

Again by using sublinear growth condition, the equations simplify to

$$\begin{aligned}
&-w^{(0)} q_{\mathrm{vs,z}}^{(0)} = C_{\mathrm{d}}^{(0)} \\
&q_{\mathrm{c},\tau}^{(1)} + u^{\infty} q_{\mathrm{c,x}}^{(1)} + u^{(0)} q_{\mathrm{c},\eta}^{(1)} = C_{\mathrm{d}}^{(0)} - C_{\mathrm{cr}}^{(0)} \\
&q_{\mathrm{r},\tau}^{(0)} + u^{\infty} q_{\mathrm{r,x}}^{(0)} + u^{(0)} q_{\mathrm{r},\eta}^{(0)} = 0
\end{aligned} \tag{B.16}$$

Undersaturated air.

$$\begin{aligned}
&q_{\mathrm{v},\tau'}^{(0)} + u^{\infty} q_{\mathrm{v},\eta}^{(0)} = 0 \\
&q_{\mathrm{v},\tau'}^{(1)} + u^{\infty} q_{\mathrm{v},\eta}^{(1)} + q_{\mathrm{v},\tau}^{(0)} + u^{\infty} q_{\mathrm{v,x}}^{(0)} + u^{(0)} q_{\mathrm{v},\eta}^{(0)} = 0 \\
&q_{\mathrm{c},\tau'}^{(1)} + u^{\infty} q_{\mathrm{c},\eta}^{(1)} = 0 \\
&q_{\mathrm{c},\tau}^{(1)} + u^{\infty} q_{\mathrm{c},\eta}^{(1)} + u^{(0)} q_{\mathrm{c},\eta}^{(1)} + q_{\mathrm{c},\tau'}^{(2)} + u^{\infty} q_{\mathrm{c},\eta}^{(2)} = -C_{\mathrm{cr}}^{(0)} \\
&q_{\mathrm{r},\tau'}^{(0)} + u^{\infty} q_{\mathrm{r},\eta}^{(0)} = 0 \\
&q_{\mathrm{r},\tau'}^{(1)} + u^{\infty} q_{\mathrm{r},\eta}^{(1)} + q_{\mathrm{r},\tau}^{(0)} + u^{\infty} q_{\mathrm{r,x}}^{(0)} + u^{(0)} q_{\mathrm{r},\eta}^{(0)} = 0
\end{aligned} \tag{B.17}$$

The equation for the evaporation source term is

$$C_{\mathrm{ev}}^{(0)} = C_{\mathrm{ev}}^{**} \left(q_{\mathrm{vs}}^{(0)}(z) - q_{\mathrm{v}}^{(0)} \right) \sqrt{q_{\mathrm{r}}^{(0)}} \tag{B.18}$$

Sublinear growth condition yields

$$\begin{aligned}
&q_{\mathrm{v},\tau}^{(0)} + u^{\infty} q_{\mathrm{v,x}}^{(0)} + u^{(0)} q_{\mathrm{v},\eta}^{(0)} = 0 \\
&q_{\mathrm{c},\tau}^{(1)} + u^{\infty} q_{\mathrm{c},\eta}^{(1)} + u^{(0)} q_{\mathrm{c},\eta}^{(1)} = -C_{\mathrm{cr}}^{(0)} \\
&q_{\mathrm{r},\tau}^{(0)} + u^{\infty} q_{\mathrm{r,x}}^{(0)} + u^{(0)} q_{\mathrm{r},\eta}^{(0)} = 0
\end{aligned} \tag{B.19}$$

Appendix C. The Adams-Bashforth timestepping reads

$$\phi^{n+1} = \phi^n + \frac{\delta t}{12}\left(23F(\phi^n) - 16\phi^{n-1} + 5F(\phi^{n-2})\right) \tag{C.1}$$

The advective derivative is discretized as

$$u^\infty \frac{\partial \phi(x_j)}{\partial x} \approx u^\infty \left[\frac{4}{3}\left(\frac{\phi_{j+1} - \phi_{j-1}}{2\delta x}\right) - \frac{1}{3}\left(\frac{\phi_{j+2} - \phi_{j-2}}{4\delta x}\right)\right] \tag{C.2}$$

For a compact notation, we introduce the following abbreviations

$$\begin{aligned}
F^n_{\bar{u}} &= -u^\infty \bar{u}^n_x \\
F^n_{\bar{w}} &= -u^\infty \bar{w}^n_x + \bar{\theta}^n \\
F^n_{\bar{\theta}} &= -u^\infty \bar{\theta}^n_x - \bar{w}^n\,(1-\sigma)\,\theta^{(2)}_z + \theta^{(2)}(w')^n + \bar{C}^n_- \\
F^n_{w'} &= -u^\infty (w')^n_x + (\theta')^n \\
F^n_{\theta'} &= -u^\infty (\theta')_x - \sigma\theta^{(2)}_z (w')^n + \sigma(1-\sigma)\bar{w}^n - \sigma\bar{C}^n_-
\end{aligned} \tag{C.3}$$

Using these, applying (C.1) to (2.23) yields the semidiscrete system

$$\begin{aligned}
\bar{u}^{n+1} &= \bar{u}^n + \frac{\delta t}{12}\left(23F^n_{\bar{u}} - 16F^{n-1}_{\bar{u}} + 5F^{n-2}_{\bar{u}}\right) - \frac{\delta t}{12}\left(23\pi^n_x - 16\pi^{n-1}_x + 5\pi^{n-2}_x\right) \\
\bar{w}^{n+1} &= \bar{w}^n + \frac{\delta t}{12}\left(23F^n_{\bar{w}} - 16F^{n-1}_{\bar{w}} + 5F^{n-2}_{\bar{w}}\right) - \frac{\delta t}{12}\left(23\pi^n_z - 16\pi^{n-1}_z + 5\pi^{n-2}_z\right) \\
\bar{\theta}^{n+1} &= \bar{\theta}^n + \frac{\delta t}{12}\left(23F^n_{\bar{\theta}} - 16F^{n-1}_{\bar{\theta}} + 5F^{n-2}_{\bar{\theta}}\right) \\
(w')^{n+1} &= (w')^n + \frac{\delta t}{12}\left(23F^n_{w'} - 16F^{n-1}_{w'} + 5F^{n-2}_{w'}\right) \\
(\theta')^{n+1} &= (\theta')^n + \frac{\delta t}{12}\left(23F^n_{\theta'} - 16F^{n-1}_{\theta'} + 5F^{n-2}_{\theta'}\right)
\end{aligned} \tag{C.4}$$

Now, an equation to compute the pressure π^n is needed. This equation is obtained by using the anelastic constraint. Define predictor values of $\bar{u}$ and $\bar{w}$ by

$$\bar{u}^{*,n} := \bar{u}^n + \frac{\delta t}{12}\left(23F^n_{\bar{u}} - 16F^{n-1}_{\bar{u}} + 5F^{n-2}_{\bar{u}}\right) - \frac{\delta t}{12}\left(-16\pi^{n-1}_x + 5\pi^{n-2}_x\right) \tag{C.5}$$

and

$$\bar{w}^{*,n} := \bar{w}^n + \frac{\delta t}{12}\left(23F^n_{\bar{w}} - 16F^{n-1}_{\bar{w}} + 5F^{n-2}_{\bar{w}}\right) - \frac{\delta t}{12}\left(-16\pi^{n-1}_z + 5\pi^{n-2}_z\right) \tag{C.6}$$

Now, by construction, it is

$$\bar{u}^{n+1} = \bar{u}^{*,n} - \frac{23\delta t}{12}\pi^n_x \tag{C.7}$$

and

$$\bar{w}^{n+1} = \bar{w}^{*,n} - \frac{23\delta t}{12}\pi^n_z \tag{C.8}$$

Multiplying both equations by $\rho^{(0)}$, applying ∂_x to (C.7) and ∂_z to (C.8), summing them and then using the anelastic constraint in (2.23) yields

$$\begin{aligned} 0 &= \left(\rho^{(0)}\bar{u}^{n+1}\right)_x + \left(\rho^{(0)}\bar{w}^{n+1}\right)_z \\ &= \left(\rho_0\bar{u}^{*,n}\right)_x + \left(\rho_0\bar{w}^{*,n}\right) - \frac{23\delta t}{12}\left[\left(\rho_0\pi_x^n\right)_x + \left(\rho_0\pi_z^n\right)_z\right] \end{aligned} \tag{C.9}$$

So the pressure π^n is computed from the elliptic equation

$$\frac{23\delta t}{12}\nabla\cdot\left(\rho^{(0)}\nabla\pi^n\right) = \nabla\cdot\left(\rho^{(0)}\left(\bar{u}^{*,n},\bar{w}^{*,n}\right)^{\mathrm{T}}\right) \tag{C.10}$$